Identification of ferroptosis-associated genes in chronic kidney disease

LISHI SHAO[1*], QIXIANG FANG[2*], CHAOFEI BA[1*], YANQING ZHANG[3],
CHEN SHI[1], YA ZHANG[4] and JIAPING WANG[1]

[1]Department of Radiology, Kunming Medical University and The Second Affiliated Hospital, Kunming, Yunnan 650500;
[2]Department of Urology, The First Affiliated Hospital of The Medical College of Xi'an Jiaotong University, Xi'an,
Shaanxi 710049; [3]Department of Radiology, Kunming Children's Hospital, Kunming, Yunnan 650034; [4]Department of
Radiology, Kunming Medical University and The Third Affiliated Hospital, Kunming, Yunnan 650500, P.R. China

Abstract. Ferroptosis serves a pivotal role in developing chronic kidney disease (CKD). The present study aimed to detect and confirm the relevance of potential ferroptosis-related genes in CKD using bioinformatics and experimentation strategies. The original GSE15072 mRNA expression dataset was retrieved from the Gene Expression Omnibus database. Subsequently, the potential differentially expressed genes associated with ferroptosis of CKD were screened using R software. Gene Ontology (GO) and Kyoto Encyclopaedia of Genes and Genomes (KEGG) pathway enrichment analyses, correlation analysis and protein-protein interactions (PPI) were performed for differentially expressed ferroptosis-associated genes (DFGs). Lastly, the expression levels of the top nine DFGs were measured in the kidney tissue of Adriamycin-induced CKD rats and healthy controls via reverse transcription-quantitative (RT-q)PCR analysis. Overall, 49 DFGs among 21 patients with CKD and nine healthy controls were identified. GO and KEGG enrichment analyses demonstrated that these DFGs were primarily involved in 'ferroptosis' and 'mitophagy'. PPI findings indicated that these ferroptosis-associated genes interacted with one another. RT-qPCR of CKD tissue from the rat model revealed that STAT3, MAPK14, heat shock protein (HSP)A5, MTOR and solute carrier family 2 member 1 (SLC2A1) mRNA levels in CKD were upregulated. Overall, 49 potential ferroptosis-associated genes of CKD were identified via bioinformatics analyses. STAT3, MAPK14, HSPA5, MTOR and SLC2A1 may influence CKD onset by regulating ferroptosis. The present results add to the existing body of knowledge about CKD and may be useful in the treatment of CKD.

Introduction

Chronic kidney disease (CKD) has become a global threat to public health. By 2040, CKD is anticipated to occupy the top five major causes of patient death (1). CKD refers to continuous renal damage and/or renal dysfunction and has high incidence rate and mortality worldwide, imposing a heavy economic and social burden (2). CKD is associated with increased risk of coronary artery disease, cardiac failure and sudden cardiac death (3). Notwithstanding progress that has been made in preventing, diagnosing and treating CKD, this disease continues to represent a notable threat to public health in the world. Therefore, there is a pressing need to develop simpler and more practical treatments for CKD.

Ferroptosis is a cell death mode that differs from apoptosis and necrosis and is induced by various small molecular substances (4). It is cell death caused by the metabolic disorder of intracellular lipid oxides and extensive reactive oxygen species (ROS) production caused by iron overload (5). Cell ferroptosis has been reported to cause endoplasmic reticulum stress and mitochondrial dysfunction in renal cells, affecting the severity and prognosis of chronic renal injury (6). Zhou *et al* (7) found that in the kidneys of patients with CKD and murine unilateral ureteral obstruction (UUO) or ischemia-reperfusion injury (IRI) model systems, expression of glutathione peroxidase 4 (GPX4) in renal tubular epithelial cells decreased while content of 4-hydroxynonenol increased. Moreover, compared with the healthy control group, inhibiting iron death notably decreases renal injury, interstitial fibrosis and inflammatory cell accumulation in UUO or IRI mice (7). However, to the best of our knowledge, ferroptosis-associated genes in CKD remain poorly characterized and require additional investigation. The investigation of the roles of these potential ferroptosis-associated genes in CKD may highlight novel biomarkers for treating this disease.

Bioinformatics is a multidisciplinary, interdisciplinary approach that integrates molecular biological analyses and

Correspondence to: Dr Jiaping Wang, Department of Radiology, Kunming Medical University and The Second Affiliated Hospital, 374 Dianmian Avenue, Kunming, Yunnan 650500, P.R. China
E-mail: jiapingwang12@163.com

*Contributed equally

technological innovation (8). It is growing into a significant computational tool to elucidate the molecular mechanism of disease (9). Furthermore, minimally invasive blood-based analysis of ferroptotic activity can offer clear insight into underlying disease status (10). In the present study, peripheral blood mononuclear cells (PBMCs) were leveraged as model targets to conduct bioenergetic analysis and monitor disease progression. PBMC samples contain a T, B and natural killer (NK) cells, as well as monocytes, that may represent ideal targets for studies of ferroptotic activity and other biosignatures of interest (11). PBMCs also reflect systemic shifts in physiological homeostasis and previous studies have explored chronic disease-associated changes in PBMC bioenergetics (12-15). In the present study, the dataset GSE15072 from the Gene Expression Omnibus (GEO) database of PBMCs of patients with CKD undergoing either conservative treatment (CKD; n=9) or haemodialysis (HD; n=12), as well as healthy controls, were analysed using bioinformatics tools. Gene Ontology (GO) and Kyoto Encyclopaedia of Genes and Genomes (KEGG) pathway enrichment analyses and correlation analyses were used to analyse the differentially expressed ferroptosis-associated genes (DFGs). Finally, expression levels of key ferroptosis genes were further verified by RT-qPCR analysis of the CKD rats and healthy renal tissue.

Materials and methods

Bioinformatics. GSE15072 mRNA profiles (GPL96 platform; Affymetrix Human Genome U133A Array; ncbi.nlm.nih. gov/geo/query/acc.cgi?acc=GSE15072) were downloaded from GEO database (ncbi.nlm.nih.gov/geo/). GSE15072 consisted of 29 samples, including eight PBMC samples from healthy controls (NORM), 9 patients with CKD and 12 with HD. The R software (r-project.org/version 3.4.0) and Bioconductor website(www.bioconductor.org/cluster-Profiler) (16,17) were utilized to identify the differentially expressed genes (DEGs). The limma package (bioconductor. org/packages/release/bioc/html/limma.html/version 3.42.2) was employed to normalize the gene expression profiles. Unpaired Student's t test was utilized to find corresponding P-values for gene symbols according to the predetermined cut-off criteria P<0.05 and |log[fold-change (FC)]|>1, thus the DEGs between patients with CKD and healthy control were determined. The heatmap was created using pheatmap package (bioconductor.org/packages/ release/bioc/html/heatmaps.html/versions/1.0.12) in R software. Furthermore, principal component analysis (PCA) (18) was conducted to verify the repeatability of the data in GSE15072. R 'ggplot2' package (http://docs.ggplot2.org/ current/Version 3.1.0) (19) was used to draw the PCA.

Screening DFGs. To identify ferroptosis-related mRNAs, 382 ferroptosis-associated genes were retrieved from the FerrDb website (http://www.zhounan.org/ferrdb/) (20). The union sets of DEGs associated with ferroptosis were validated by a Venn diagram analysis using the Interacti-Venn website (bioinfogp. cnb.csic.es/tools/venny/index. html/version 2.1) (21). The heatmap and PCA were used for analysing ferroptosis-associated genes (Table SI), as aforementioned. Subsequently, R 'ggplot2'

package((http://docs.ggplot2.org/current/Version 3.1.0) (19) was used to draw the box plot.

GO and KEGG analysis. The GO((http://www.geneontology. org/) (22) and KEGG((http://www.genome.jp/kegg/) (23) enrichment were used for ferroptosis-associated gene function analyses. Analysed GO terms included molecular function (MF), cellular component (CC) and biological process (BP).

Immune infiltration analysis. The CIBERSORT algorithm (cibersort.stanford.edu/) (24) was applied to examine the ferroptosis-associated genes and the ratio of 20 immunological cell types such as M0/M1/M2 macrophages, eosinophils, neutrophils, γδT, regulatory T (Treg), naïve, resting and activated memory CD4$^+$ T cells, as well as monocytes CD8$^+$ T, naïve and memory B, resting and activated NK, resting mast, plasma and resting and activated dendritic cells were obtained. Moreover, the association between prognostic genes and immune cells was assessed via Spearman's correlation test.

Protein-protein interaction (PPI) and correlation analyses of DFGs. The interaction among ferroptosis-associated genes was examined using STRING online database (https://string-db. org/version 11.0) and Cytoscape (manual.cytoscape.org/ version 3.8.1; Cytoscape Consortium, San Diego, CA, USA) (25). DFG correlations were analysed using the 'Corrplot' package ((https://github.com/taiyun/corrplot) in R software (Spearman correlation analysis).

Animals. National Institutes of Health guidelines (26) were followed to conduct animal studies with pre-approval of the Animal Ethical and Welfare Committee of Kunming Medical University (approval no. Kmmu20221379). Male Sprague-Dawley (SD) rats of 6 weeks of age (180-200 g) were purchased from the Experimental Animal Center of Kunming Medical University [specific-pathogen-free; license no. SYXK (Dian) k2020-0006] and were housed under standard conditions (12/12-h light/dark cycle; 22-25°C; 50-60% humidity). During the period of the experiment, these rats took food and water freely.

Animal model. A total of 22 male SD rats were randomized into healthy control and CKD groups, with 11 rats in each group. CKD model rats were prepared as described below. Anesthetization was induced by inhalation of 2.5% isoflurane and was maintained with 1.5% isoflurane. Rats were intravenously injected via the tail vein with Adriamycin (3.5 mg/kg in saline; Sigma-Aldrich; Merck KGaA). After two weeks, a second dose of the Adriamycin solution was administered. In addition, healthy control group received an equal volume normal saline injections. After 8 weeks from the final administration, blood urea nitrogen (BUN) and serum creatinine (Scr) were quantified to assess successful model generation. Then 2.5% isoflurane was used to anesthetize rats prior to euthanasia via cervical dislocation. After rats had ceased breathing, the hearts were no longer beating and paws and eyeballs had turned white, their left renal tissue was harvested. Each left kidney was split into two, with one portion undergoing 4% paraformaldehyde fixation before histological analysis and the other being snap-frozen with liquid nitrogen before storage at -80°C.

Table I. Primer sequences.

Gene	Forward	Reverse
STAT3	5'-TTAACATTCTGGGCACGAACA-3'	5'-TGACAATCAAGGAGGCATCAC-3'
JUN	5'-TGGGCACATCACCACTACACC-3'	5'-GAAGTTGCTGAGGTTGGCGTAG-3'
MTOR	5'-ACCCTCCATCCACCTCATCAG-3'	5'-CCTGGTCATTCAGAGCCACAAA-3'
VEGF	5'-GCACTGGACCCTGGCTTTACT-3'	5'-AACTTCACCACTTCATGGGCTTT-3'
HMOX1	5'-CACAGGGTGACAGAAGAGGCT-3'	5'-TCTGTGAGGGACTCTGGTCTTTG-3'
HSPA5	5'-TTCTGCTTGATGTGTGTCCTCTTAC-3'	5'-CACCTTCGTAGACCTTGATTGTTAC-3'
MAPK14	5'-CCCGAGCGATACCAGAACCT-3'	5'-TGGCGTGAATGATGGACTGA-3'
ATF3	5'-GGGTCACTGGTGTTTGAGGATT-3'	5'-TTTGTTTCTTTCCCGCCG-3'
SLC2A1	5'-AGGAGATGAAAGAAGAGGGTCG-3'	5'-GTGTTGACGATACCCGAGCC-3'
GAPDH	5'-CTGGAGAAACCTGCCAAGTATG-3'	5'-GGTGGAAGAATGGGAGTTGCT-3'

Histological analysis. Following fixation overnight using 4% paraformaldehyde at room temperature, renal tissue samples were paraffin-embedded, cut into 4-μm slices and deparaffinized with ascending series of alcohol (95, 90, 80 and 70% alcohol each 10 min). For H&E staining (Wuhan Servicebio Technology Co., Ltd.), the sections were stained with hematoxylin for 1 min and eosin for 20 sec at room temperature, and then washed with tap water. Next, the sections were dehydrated in 100% alcohol, permeabilized with xylene and mounted with neutral gum. For Masson staining (Wuhan Servicebio Technology Co., Ltd.), the sections were soaked in Masson A overnight and rinsed with tap water. Next, Masson B, Masson C were prepared into Masson solution according to the ratio of 1:1. Then, the sections were stained with Masson solution for 1 min. After washing with running water, the sections were differentiated with 1% hydrochloric acid alcohol and rinsed with tap water. The sections were then treated with Masson D for 6 min, washed with tap water, immersed in a Masson E for 1 min and Masson F for 2-30s. Sections were rinsed with 1% glacial acetic acid and then dehydrated with anhydrous ethanol. Finally, the sections were immersed with xylene and sealed with neutral gum. For PAS staining (Wuhan Servicebio Technology Co., Ltd.), the sections were stained with PAS dye solution B for 10-15 min, rinsed with tap water, and then rinsed twice with distilled water. Next, the sections were stained with PAS A for 25-30 min in the dark and rinsed with tap water for 5 min. Then the sections were stained with PAS C for 30s and rinsed with tap water. Subsequently, the sections were treated with Hydrochloric acid solution and Ammonia, each step required washing with distilled water. Then the sections were dehydrated with alcohol and xylene and mounted in neutral gum. Morphological changes in the renal tissues were evaluated using an Olympus light microscope (magnification, x400; Olympus Corporation).

RT-qPCR. Total RNA in kidney tissue was extracted using RNA Extracting Solution (Wuhan Servicebio Technology Co., Ltd. G3013) according to the manufacturer's instructions. Total RNA (1 μg) was reverse transcribed into cDNA using the RevertAid reverse transcriptase kit (Wuhan Servicebio Technology Co., Ltd.) under the following conditions: 25˚C for 5 min, 42˚C for 30 min and 85˚C for 5 sec. qPCR was performed using 2X SYBR Green qPCR Master Mix kit (Wuhan Servicebio Technology Co., Ltd. G3320). Thermocycling conditions for PCR were: Pre-incubation at 95˚C for 30 sec; 40 cycles of 95˚C for 15 sec, annealing 60˚C for 30 sec. Subsequently, 2.0% agarose gel electrophoresis was used to separate PCR amplicons, which underwent densitometric analysis. Applied Biosystems 7300 real-time PCR system (Applied Biosystems; Thermo Fisher Scientific, Inc.) and software (7500 Fast System SDS Software version 1.4) were used with primers for STAT3, Jun kinase (JUN), Mechanistic target of rapamycin (MTOR), vascular endothelial-derived growth factor (VEGF), Heme oxygenase 1 (HMOX1), Heat shock protein A5 (HSPA5), Mitogen-activated protein kinase 14 (MAPK14), activation transcription factor 3 (ATF3), solute carrier family 2 member 1 (SLC2A1), and GAPDH, as listed in Table I. mtDNA levels were quantified using the 2-$\Delta\Delta$Cq method for triplicate samples with GAPDH as the internal reference (27).

Statistical analysis. All experiments were performed in triplicate. Data are expressed as the mean ± standard deviation. R (version 3.6.2 x64; R Foundation for Statistical Computing) (28) was used for statistical analyses. Unpaired Student's t test was used to analyse gene expression levels of the animal samples with SPSS version 23.0 (IBM Corp.). $P<0.05$ was considered to indicate a significant difference.

Results

Validation of DFGs in COPD Patients. DFGs were identified following batch correction and microarray standardization for GSE15072. A total of 2,247 DFGs were identified, consisting of 1,238 up- and 1,009 downregulated genes (Fig. 1B). The heatmap in Fig. 1A presents the expression levels of DFGs. PCA was performed to examine the repeatability of intra-group data, which revealed that the data in GSE15072 had good repeatability (Fig. 1C). By taking the intersection of ferroptosis-related genes and DEGs, 49 DFGs were identified between CKD and normal groups (Fig. 1D and E). PCA of DFGs is displayed in Fig. 1F. Moreover, box plots demonstrated the expression of 49 DFGs in CKD and normal samples (Fig. 2). The top five up-regulated genes of the CKD
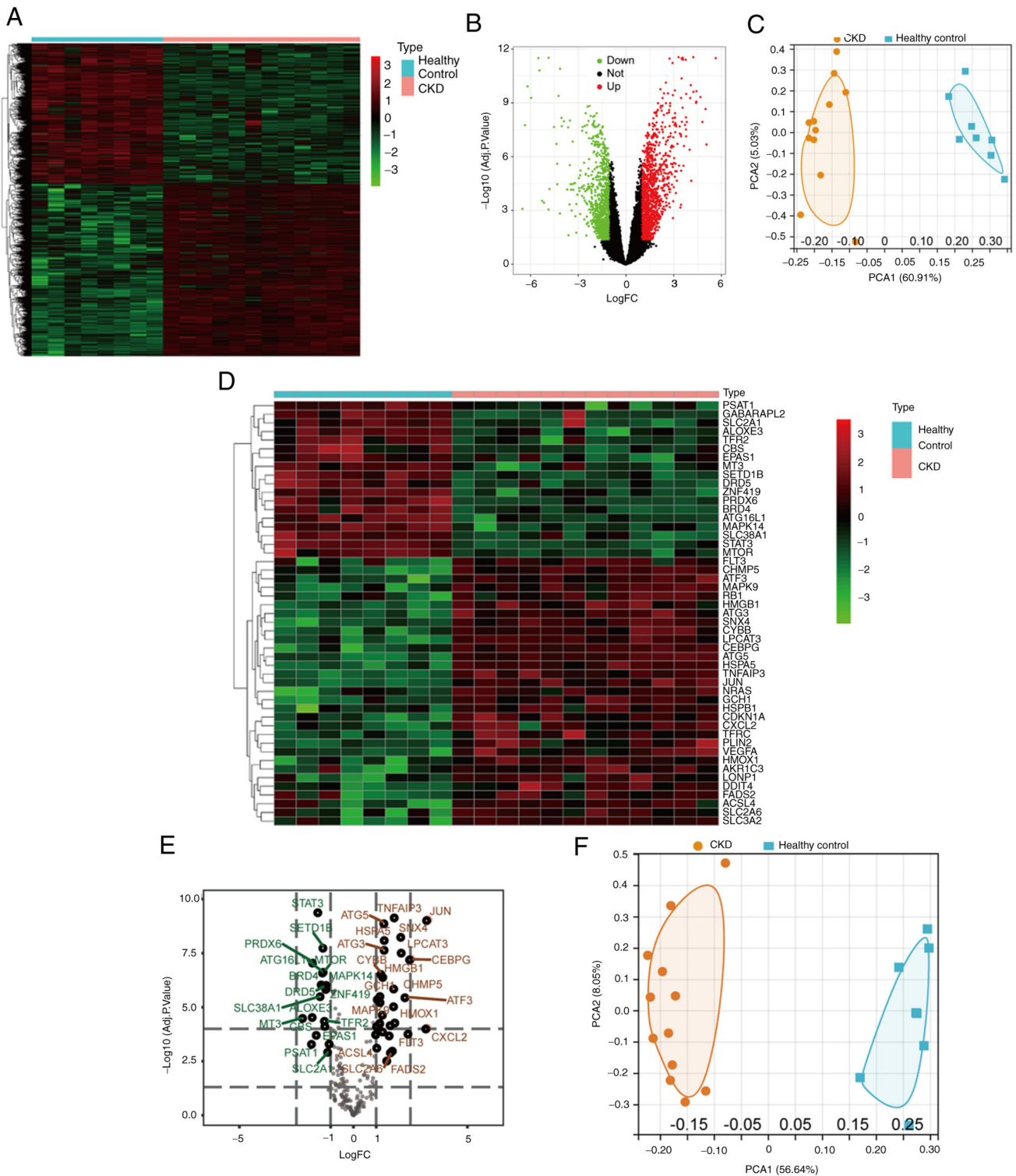
Figure 1. Bioinformatics analysis of differential gene expression. (A) Heatmap, (B) volcano plots and (C) PCA of gene expression of CKD in GSE5406. (D) Heatmap, (E) volcanic plots and (F) PCA of 49 differentially expressed ferroptosis-associated genes. PCA, principal component analysis; Adj.P.val, adjusted P-value; CKD, chronic kidney disease.

group included aldo-keto reductase 1C3, ATF3, antithymocyte globulin 3 (ATG3), ATG5 and cyclin-dependent kinase inhibitor 1 (CDKN1A), and the top five downregulated genes included arachidonate lipoxygenase 3 (ALOXE3), autophagy related 16 like 1 (ATG16L1), bromodomain-containing protein 4 (BRD4), cystathionine β-synthase (CBS), and dopamine receptor D5 (DRD5) (Fig. 2).

Pathway enrichment analysis of DFGs. To explore the biological roles of these DFGs, GO and KEGG enrichment analysis was conducted using R software. This approach demonstrated that the most significantly enriched GO terms were involved in 'response to nutrient levels', 'cellular response to extracellular stimulus' and 'ROS metabolic process' (BP), 'melanosome', 'pigment granule' and 'autophagosome' (CC) and 'ubiquitin
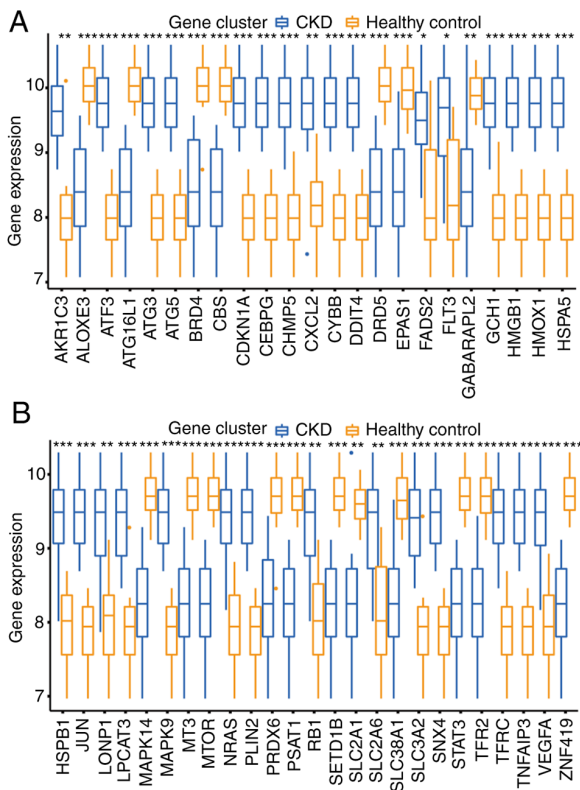
Figure 2. Boxplot of 49 DFGs in CKD and healthy samples. (A) Boxplot of the top 25 DFGs in CKD and healthy control samples. (B) Boxplot of the bottom 24 DFGs in CKD and healthy control samples. *P<0.05, **P<0.001 and ***P<0.001 vs. healthy control. DFGs, differentially expressed ferroptosis-associated genes; CKD, chronic kidney disease.

protein ligase binding', 'ubiquitin-like protein ligase binding' and 'protein self-association' (MF; Fig. 3). In KEGG enrichment analysis, DFGs were primarily involved in 'ferroptosis' and 'Kaposi sarcoma-associated herpesvirus infection' (Fig. 4). The KEGG pathway annotation of 'ferroptosis' is presented in Fig. 5.

PPI and correlation analysis of DFGs. To determine the interactions between DFGs, a PPI network was constructed. These findings showed that the ferroptosis-associated genes interacted with one another (Fig. 6A) and revealed interaction numbers for individual genes (Fig. 6B). As STRING database does not completely cover all genes, only 40 DFGs could be analysed. To examine expression correlation between these DFGs, correlation analysis was performed. Fig. 7 shows the association between 49 DFGs in the GSE15072 dataset.

Immune infiltration assessment. To the best of our knowledge, due to technical limitations, such as integration and search of genomic information (29), the immune landscape in CKD remains to be fully elaborated, particularly in a low abundance of cell subpopulations. Using immune score P<0.05, 20 samples were screened for immune analysis. To study differences in immune infiltration between patients with CKD and healthy controls in 20 immune cell types, the CIBERSORT algorithm was used. Fig. 8A displays the results obtained from eight healthy controls and 21 patients with CKD. Compared with normal tissue, CKD tissue generally exhibited more plasma cells, resting memory CD4$^+$ T, γδT, resting and activated NK

cells as well as monocytes. By contrast, the proportions of naive B and CD4$^+$ T and Tregs, as well as M0 macrophages and neutrophils, were lower (Fig. 8B).

Correlation between DFG expression and immune infiltration in CKD. It is unclear if DFGs influence immune cell recruitment in the CKD microenvironment. Therefore, the present study analysed the association between ferroptosis-related genes and immune infiltration in CKD. The immune infiltration level of naive CD4$^+$ T cells was positively associated with expression of SET domain-containing 1B (SETD1B), MTOR and SLC38A1 (Fig. 9). The immune infiltration of γδT cells was positively associated with ATF3 and JUN expression levels (Fig. 9). Immune infiltration of Tregs was positively correlated with MT3 and MTOR levels (Fig. 9). The immune infiltration of monocytes was positively correlated with antithymocyte globulin 3 (ATG3), ATG5, CDKN1A, CCAAT enhancer binding protein (CEBPG), charged multivesicular body protein 5 (CHMP5), Cytochrome b-245 beta chain (CYBB), DDIT4 (DNA damage inducible transcript 4), GCH1 (GTP cyclohydrolase 1), high mobility group box 1 (HMGB1), HMOX1, HSPA5), MAPK9, neuroblastoma RAS viral oncogene homolog (NRAS), retinoblastoma susceptibility gene (RB1), SLC3A2), sorting nexin-4 (SNX4), TNF-alpha-induced protein 3 (TNFAIP3) and VEGFA) expression, but negatively correlated with arachidonate lipoxygenase 3 (ALOXE3), autophagy related 16 like 1 (ATG16L1), BRD4, DRD5), endothelial PAS Domain Protein 1 (EPAS1), MAPK14, metallothionein-3 (MT3), MTOR), phosphoserine aminotransferase 1 (PSAT1), SETD1B, SLC38A1), STAT3, transferrin receptor 2 (TFR2) and zinc Finger Protein 419 (ZNF419) (Fig. 10). The immune infiltration of neutrophils was positively associated with expression of ALOXE3, ATG16L1, BRD4, CBS, DRD5, EPAS1, MAPK14, MT3, MTOR, peroxiredoxin 6 (PRDX6), PSAT1, SETD1B, SLC38A1, STAT3, TFR2 and ZNF419, whereas it was negatively correlated with antithymocyte globulin 3 (ATG3), ATG5, CDKN1A, CCAAT enhancer binding protein (CEBPG), charged multivesicular body protein 5 (CHMP5), CYBB, DNA damage inducible transcript 4 (DDIT4), GTP cyclohydrolase 1 (GCH1), high mobility group box 1 (HMGB1), HMOX1, HSPA5, HSPB1, Lon protease 1 (LONP1), lysophosphatidylcholine acyltransferase 3 (LPCAT3), MAPK9, SLC3A2, SNX4 and TNFAIP3 (Fig. 11). CDKN1A and CXC motif chemokine ligand 2 (CXCL2) levels were negatively associated with levels of resting NK cells (Fig. 12). A positive association between activated NK cells and CDKN1A, activated dendritic cells and GABA type A receptor-associated protein 2 and plasma cells and HMOX1 expression was found in this analysis (Fig. 12). Moreover, M0 macrophages were positively associated with expression of CBS, EPAS1 and TFR2 (Fig. 12). The present results suggested that DFGs were associated with immune infiltration in CKD.

Validating DFGs in CKD. To confirm GSE15072 dataset reliability, the expression of the top nine DFGs was assessed in the CKD animal model via RT-qPCR. To confirm that the present CKD model rat accurately recapitulated the features of this disease, levels of BUN and Scr in these animals were measured (Fig. 13A and B). This analysis found that Adriamycin induced a significant decrease in renal function, characterized
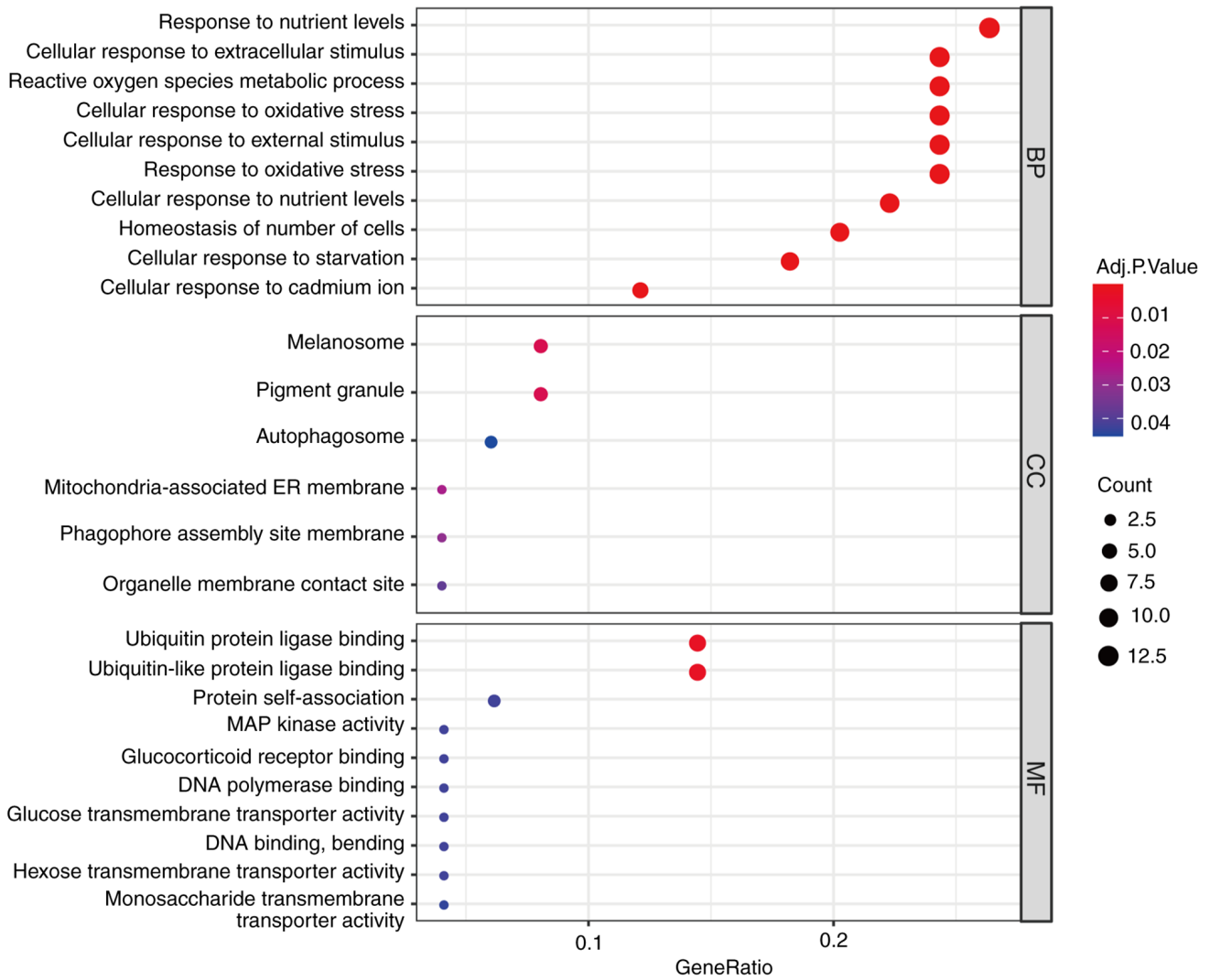
Figure 3. GO enrichment analysis of 49 differentially expressed ferroptosis-associated genes. B bubble plot of enriched GO terms. GO, Gene Ontology; BP, biological process; CC, cellular component; MF, molecular function.
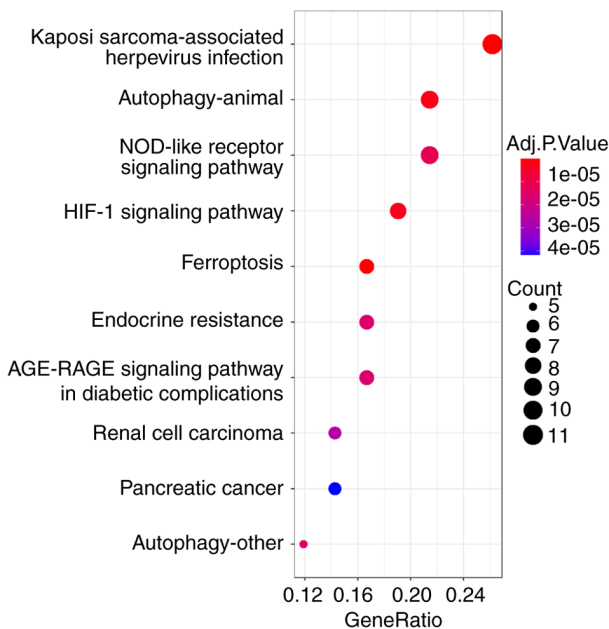

Figure 4. Kyoto Encyclopedia of Genes and Genomes analysis of 49 differentially expressed ferroptosis-associated genes.

by increased BUN and Scr levels (P<0.001). Subsequently, the effect of Adriamycin on renal tissue morphology was considered by analysing H&E and PAS-stained tissue sections (Fig. 13C and D). Relative to healthy controls, kidney samples from CKD group animals exhibited focal glomerular sclerosis in some glomerular and interstitial lesions, interstitial inflammatory infiltrate, tubular dilatation and atrophy and adenine crystalline deposits. Furthermore, Masson's trichrome stain of CKD rats displayed collagen fibril accumulation (blue) in the tubulointerstitium (Fig. 13E).

The aforementioned results suggested that a well-characterized model of CKD was successfully established. RT-qPCR, results shown that the expression levels of STAT3, MAPK14, HSPA5, MTOR and SLC2A1were significantly higher in CKD rats compared with normal kidney samples (Fig. 14). However, expression of JUN, VEGF, HMOX1 and ATF3 was not significantly different between these groups (Fig. 14).

Discussion

Ferroptosis is regulated by a series of factors and signalling pathways linked with various metabolic changes, such as
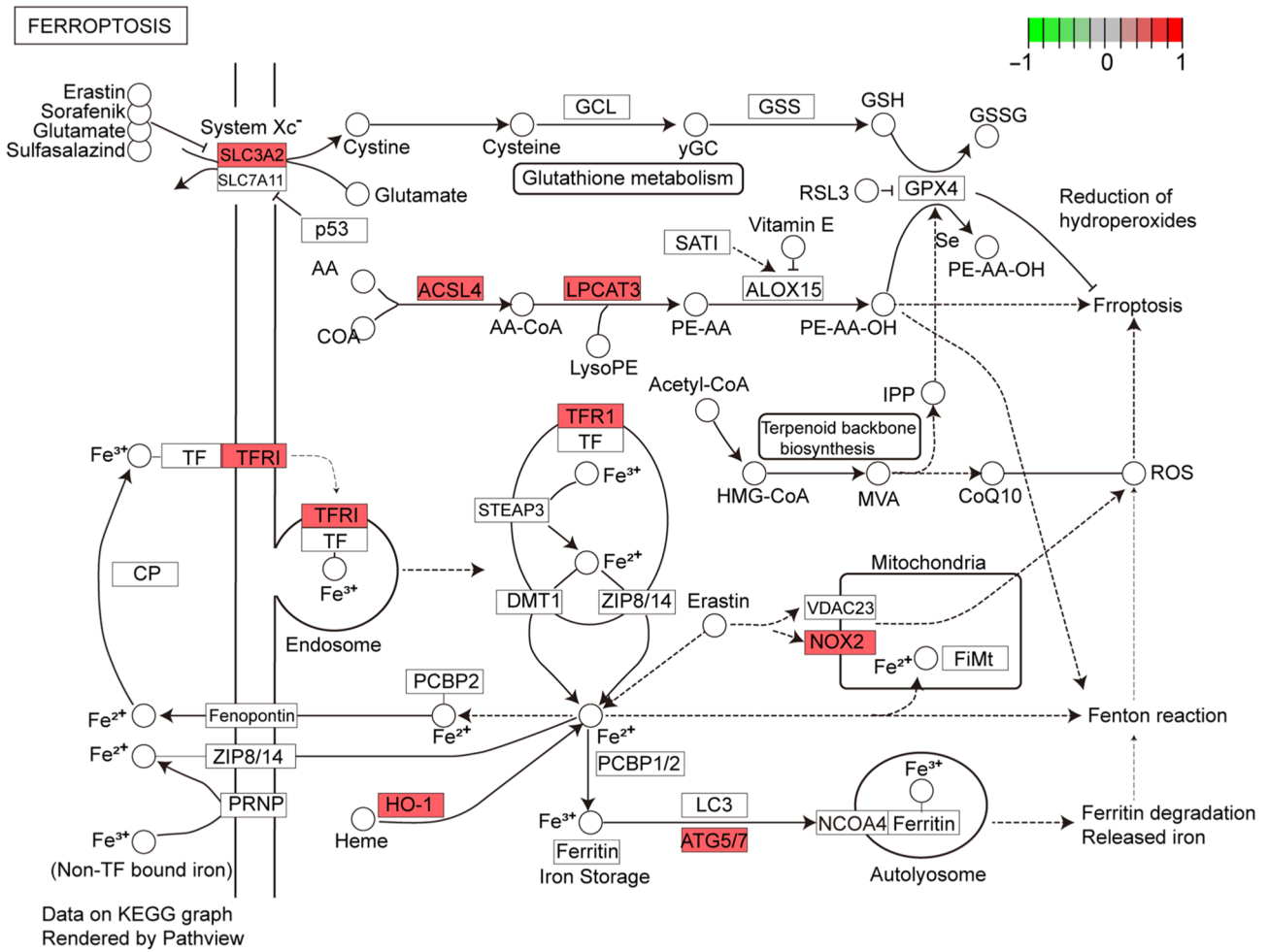
Figure 5. KEGG pathway analysis of 'ferroptosis'. Red represents the leading edge genes of hub genes. KEGG, Kyoto Encylcopedia of Genes and Genomes.
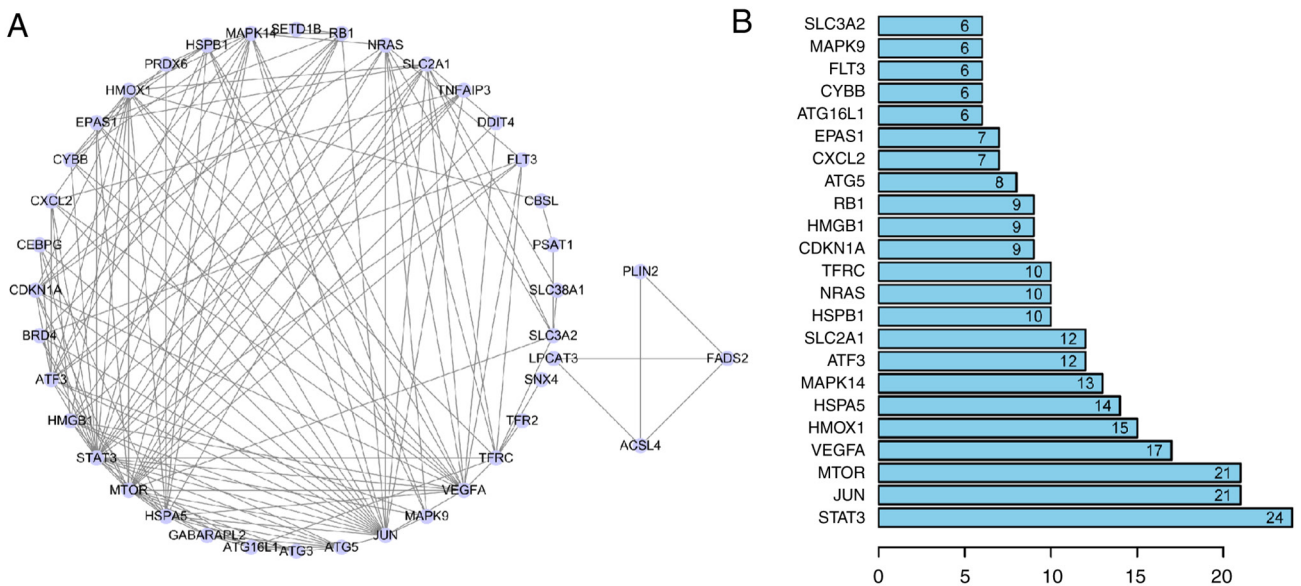

Figure 6. PPI analysis of 40 DFGs. (A) PPI of 40 DFGs. (B) Interaction number of DFGs. DFGs, differentially expressed ferroptosis-associated genes; PPI, protein-protein interaction.

abnormal amino acid metabolism, iron accumulation and subsequent lipid peroxidation (6). Iron deposition has been proven to iron uptake increase and/or iron export impairment in the kidneys of patients with CKD (30), which suggests that
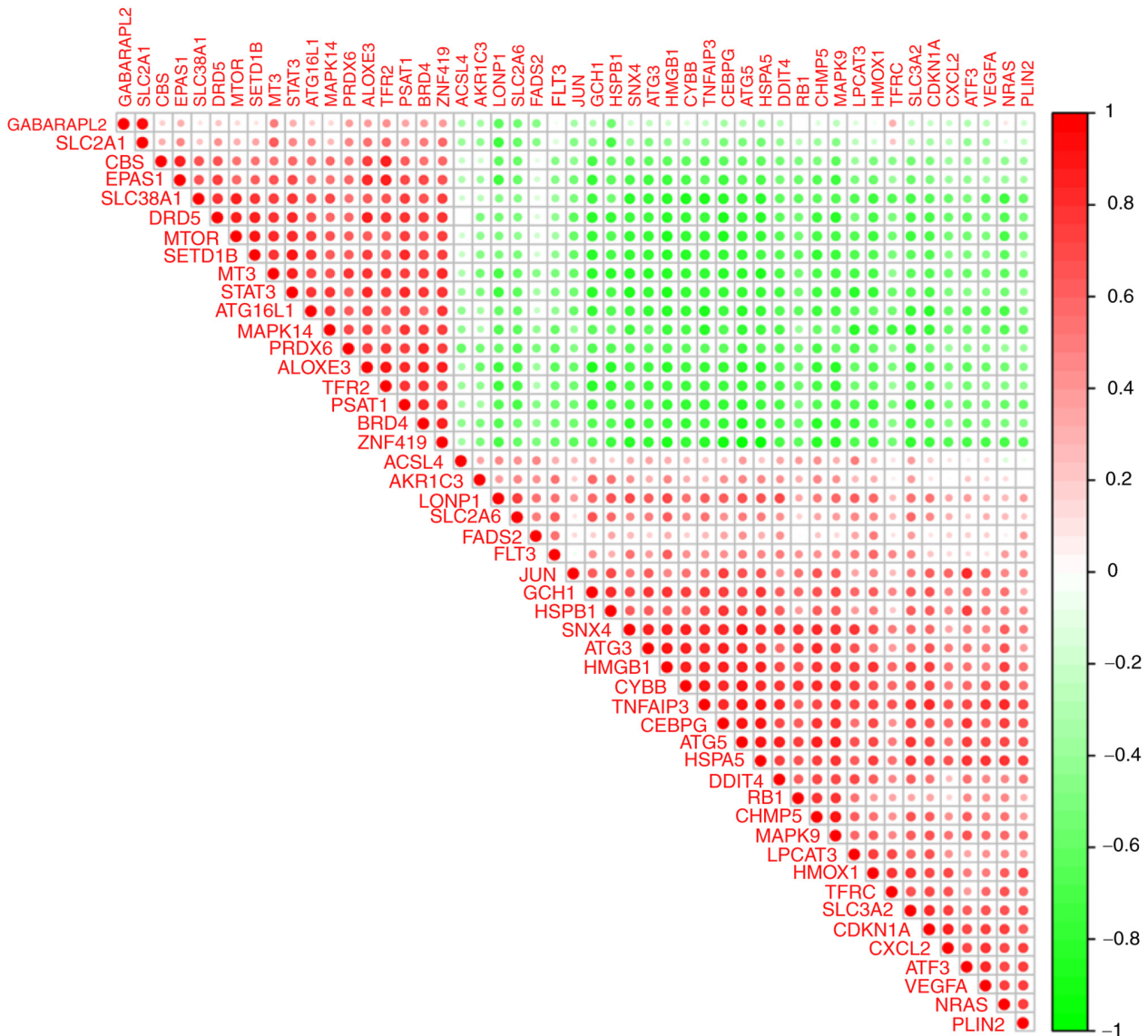
Figure 7. Spearman correlation analysis of 49 differentially expressed ferroptosis-associated genes.

the CKD-associated renal iron accumulation may first induce ferroptosis, with iron playing a detrimental role in CKD. The present study investigated the key ferroptosis-associated regulatory genes in PBMCs isolated from patients with CKD. These findings clarify the correlation between ferroptosis and CKD, which may help screen novel biomarkers for the early diagnosis and treatment of CKD.

In the present study, DFGs of CKD were first determined by comparing the gene expression profiles of healthy controls and patients with CKD. A total of 49 CKD-associated ferroptosis genes were found, which revealed that ferroptosis-associated genes were involved in CKD pathogenesis, providing potential pharmacological targets. Functions of the identified DFGs were explored by GO and KEGG enrichment analysis. Moreover, GO and KEGG analyses revealed that these 49 DFGs were primarily associated with 'response to nutrient levels', 'autophagy', 'HIF-1 signalling pathway', 'ferroptosis', 'lipid' and 'atherosclerosis'. These pathways were involved in CKD. Previous studies indicated that ferroptosis is important in apoptosis of renal tubular epithelial cells and

epithelial-mesenchymal transition of renal tubular cells (31-33). Zhao *et al* (34) discovered that hypoxia-inducible factor-1 activate Notch-1 transcriptionally and post-transcriptionally and promotes renal fibrosis in a cisplatin-induced mouse CKD model. Targeted inhibition of kidney cells ferroptosis in patients with CKD may be a novel direction for the therapy of CKD.

The STRING database was used to generate DFG PPI networks and nine hub genes for ferroptosis in CKD were identified by Cytoscape software: STAT3, JUN, MTOR, VEGF, HMOX1, HSPA5, MAPK14, ATF3 and SLC2A1. For bioinformatics, the top nine DFGs were validated via RT-qPCR in the kidney of the CKD rat model. This confirmed that STAT3, MAPK14, HSPA5, MTOR and SLC2A1 levels in the kidney of the CKD animal model were significantly increased compared with those in the normal controls. STAT3 plays a key role in tumorigenesis and inflammation (35). Its activation via phosphorylation increases lysosomal membrane permeability and promotes survival of breast cancer cells in the context of erastin-induced ferroptosis (36). MAPK14 is a
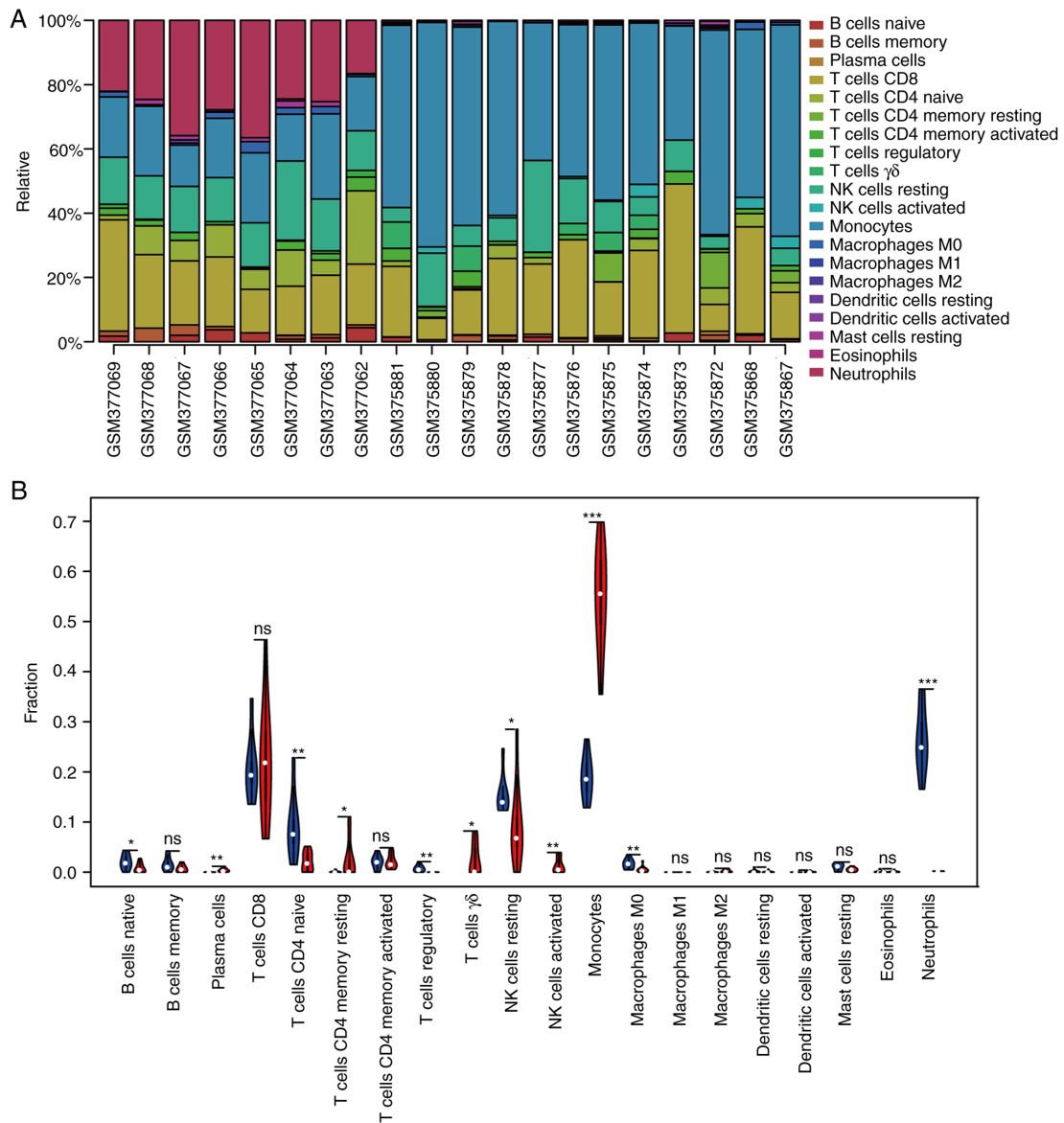
Figure 8. Immune infiltration comparison of patients with CKD (red) and normal controls (blue). (A) Relative percentage of 20 subpopulations of immune cells in 20 samples from the GSE15072 dataset. (B) Immune infiltration differences in CKD and normal control samples. *P<0.05, **P<0.001, ***P<0.001 vs. healthy control group. CKD, chronic kidney disease; NK, natural killer; ns, not significant.
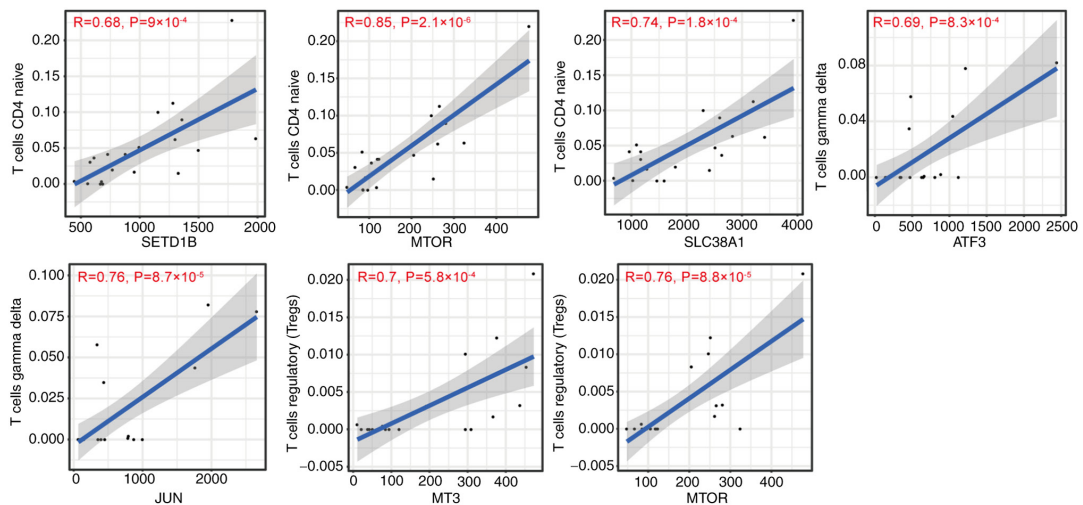

Figure 9. Correlation between ferroptosis-associated gene expression and immune infiltration of CD4+ T, γδT and regulatory T cells in chronic kidney disease. SETD1B, SET domain-containing 1B; SLC38A1, solute carrier Family 38 Member 1; ATF3, activating Transcription Factor 3; MT3, metallothionein 3.
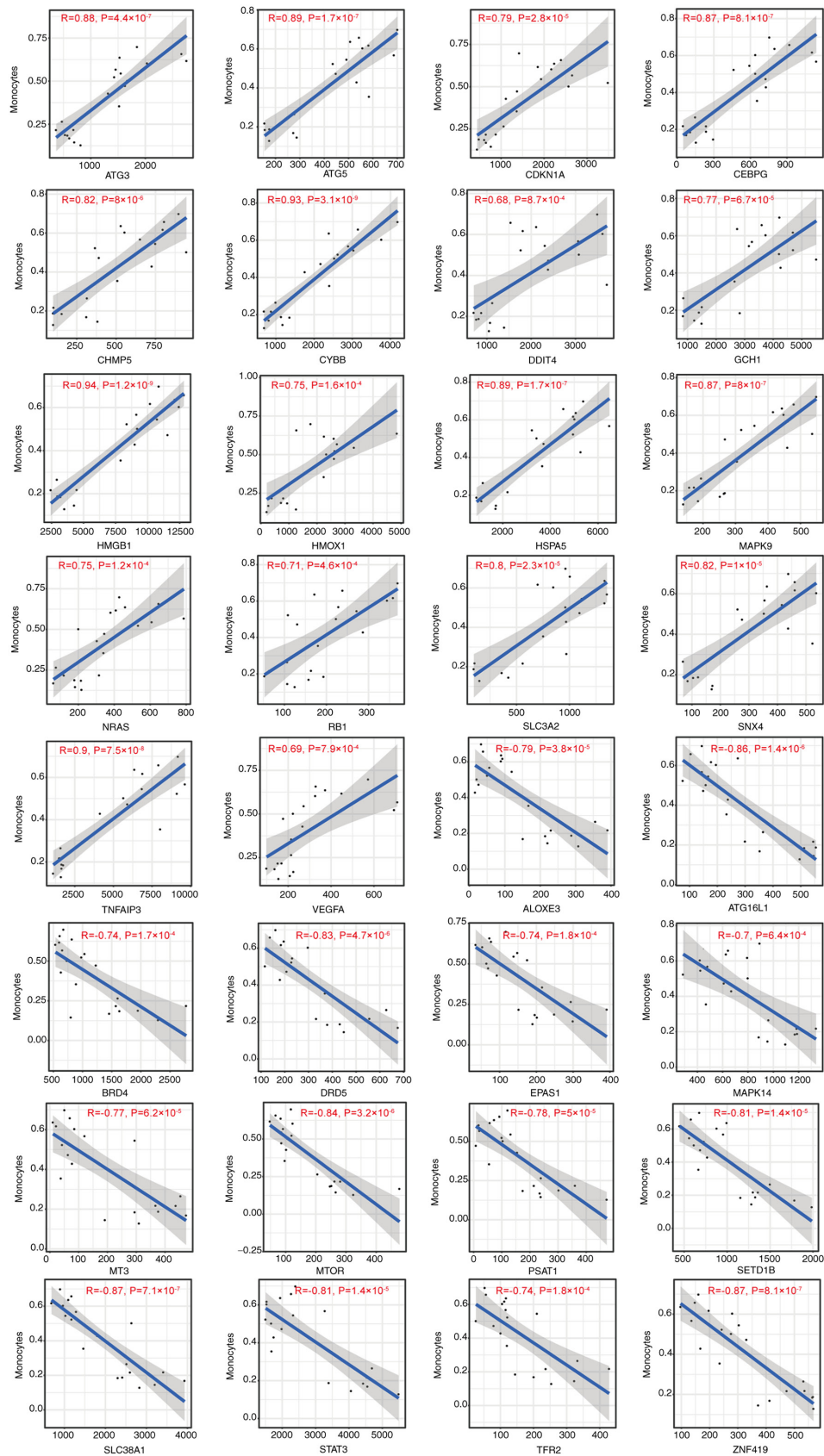
Figure 10. Correlation between ferroptosis-associated gene expression and the immune infiltration of monocytes in chronic kidney disease. ATG, antithymocyte globulin; CDKN1A, cyclin-dependent kinase inhibitor 1; CEBPG, CCAAT enhancer binding protein; CHMP5, charged multivesicular body protein 5; CYBB, Cytochrome b-245 beta chain; DDIT4, DNA damage inducible transcript 4; GCH1, GTP cyclohydrolase 1; HMGB1, high mobility group box 1; HMOX1, heme oxygenase 1; HSPA5, heat shock protein 5; NRAS, neuroblastoma RAS viral oncogene homolog; RB1, retinoblastoma susceptibility gene; SLC3A2, solute carrier 3A2; SNX4, sorting nexin-4; TNFAIP3, TNF-α-induced protein 3; VEGFA, vascular endothelial-derived growth factor; ALOXE3, arachidonate lipoxygenase 3; ATG16L1, autophagy related 16 like 1; BRD4, bromodomain-containing protein 4; DRD5, dopamine receptor D5; EPAS1, endothelial PAS Domain Protein 1; MT3, metallothionein-3; PSAT1, phosphoserine aminotransferase 1; SETD1B, SET domain-containing 1B; TFR2, Transferrin receptor 2; ZNF419, zinc finger Protein 419.
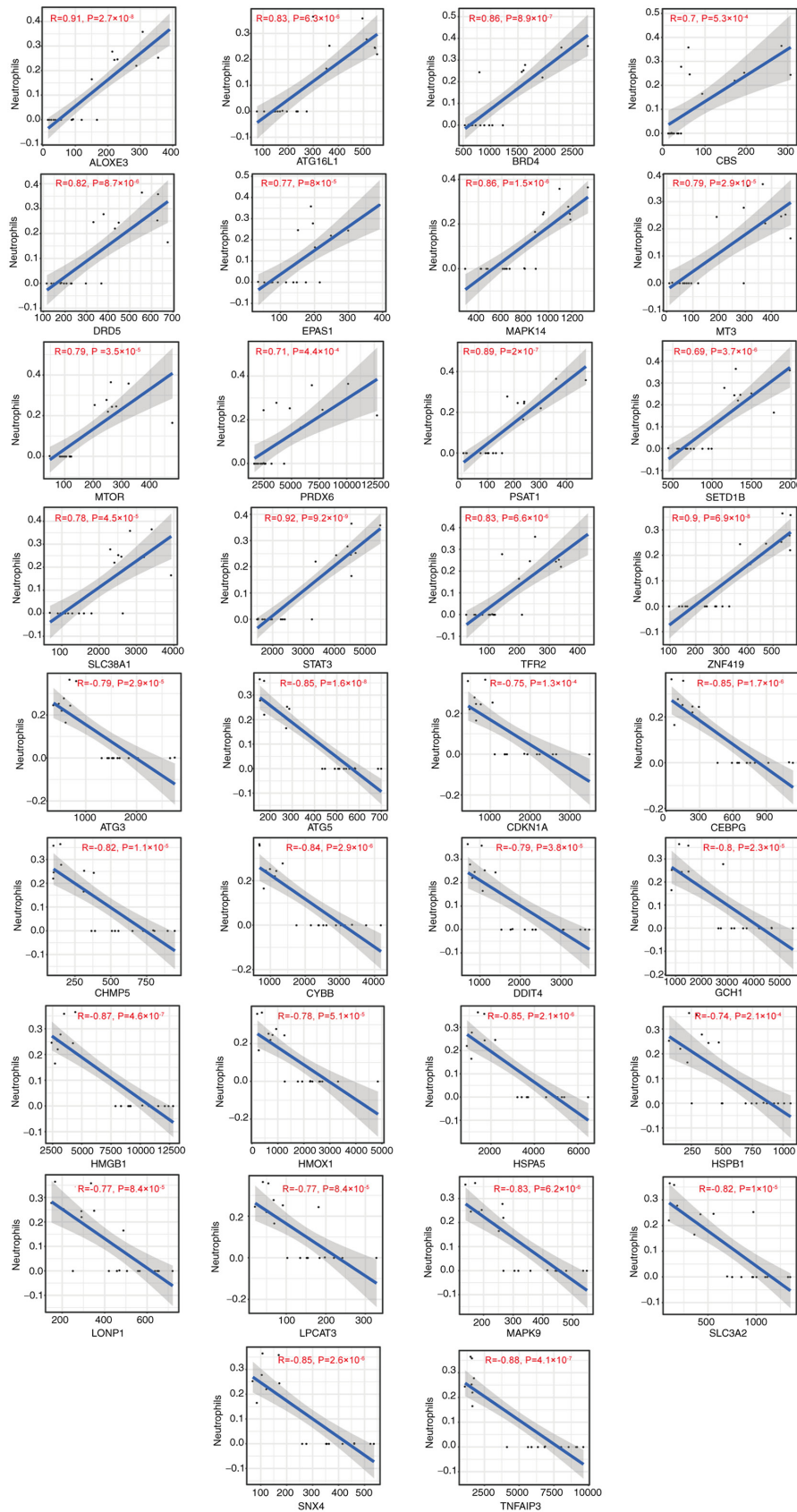
Figure 11. Correlation between ferroptosis-associated gene expression and immune infiltration of neutrophils in chronic kidney disease. ATG, antithymocyte globulin; CDKN1A, cyclin-dependent kinase inhibitor 1; CEBPG, CCAAT enhancer binding protein; CHMP5, charged multivesicular body protein 5; CYBB, Cytochrome b-245 beta chain; DDIT4, DNA damage inducible transcript 4; GCH1, GTP cyclohydrolase 1; HMGB1, high mobility group box 1; HMOX1, heme oxygenase 1; HSP5, heat shock protein 5; NRAS, neuroblastoma RAS viral oncogene homolog; RB1, retinoblastoma susceptibility gene; SLC3A2, solute carrier 3A2; SNX4, sorting nexin-4; TNFAIP3, TNF-α-induced protein 3; VEGFA, vascular endothelial-derived growth factor; ALOXE3, arachidonate lipoxygenase 3; ATG16L1, autophagy related 16 like 1; BRD4, bromodomain-containing protein 4; DRD5, dopamine receptor D5; EPAS1, endothelial PAS Domain Protein 1; MT3, metallothionein-3; PSAT1, phosphoserine aminotransferase 1; SETD1B, SET domain-containing 1B; TFR2, Transferrin receptor 2; ZNF419, zinc Finger Protein 419; CBS, cystathionine β-synthase; PRDX6, peroxiredoxin 6; LONP1, Lon protease 1.
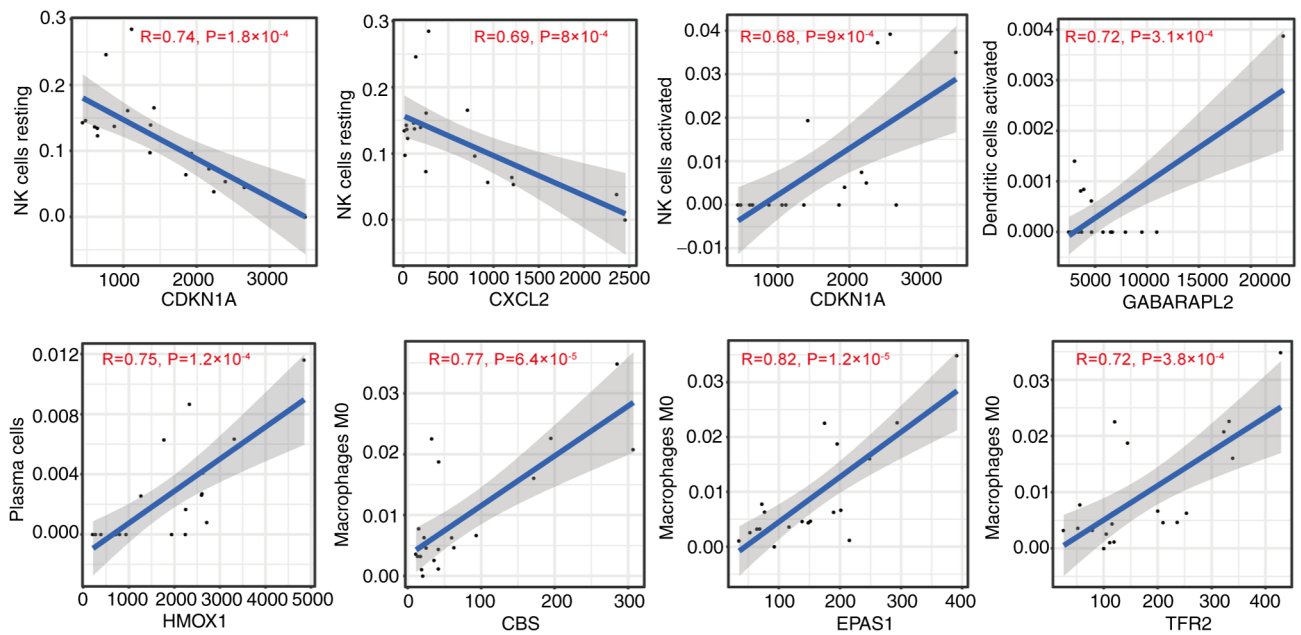
Figure 12. Correlation between ferroptosis-associated gene expression and the immune infiltration of NK, dendritic and plasma cells and M0 macrophages in chronic kidney disease. NK, natural killer; CDKN1A, cyclin-dependent kinase inhibitor 1; CXCL2, CXC motif chemokine ligand 2; GABARAPL2, GABA type A receptor-associated protein 2; HMOX1, heme oxygenase 1; CBS, cystathionine β-synthase; EPAS1, Endothelial PAS Domain Protein 1; TFR2, transferrin receptor 2.
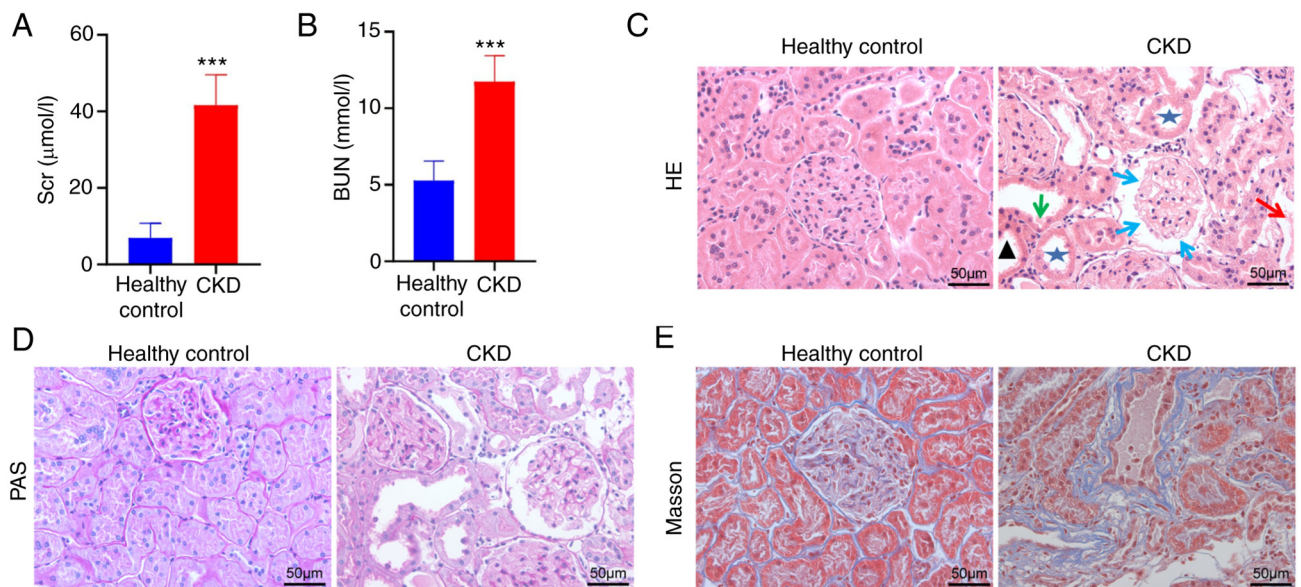

Figure 13. Adriamycin-induced CKD rat model. Levels of (A) Scr and (B) BUN in the groups (n=11). Data are presented as the mean ± standard deviation. ***P<0.001 vs. healthy control. (C) Changes in kidney morphology as assessed via HE staining. (D) Representative images of PAS staining. Light microscopy images following HE and PAS staining show notably increased brush border loss in renal tubules (green arrows), tubular necrosis (red arrows), tubular dilatation (asterisk), the formation of protein casts (black triangle) and Bowman's capsule dilatation (blue arrows). (E) Masson's trichrome staining of fibrotic regions in the renal parenchyma (blue). CKD, chronic kidney disease; PAS, periodic acid-Schiff; BUN, blood urea nitrogen; Scr, serum creatinine; HE, hematoxylin and eosin.

key part of the MAP kinase signal transduction pathway, which is crucial for mitophagy (37). HSPA5 directly protects cells from endoplasmic reticulum stress due to ROS damage (38). The atypical serine/threonine kinase mTOR is a key cell proliferation and metabolism regulator. mTOR accelerates anabolic processes such as nucleotide, fatty acid, ribosome biogenesis and protein and lipid synthesis and inhibits catabolic processes such as autophagy (39). SLC2A1 encodes

glucose transporter-1 (GLUT1), which is the primary glucose transport protein present in the blood-brain barrier (40). To the best of our knowledge, however, how these genes influence CKD pathogenesis remains unclear and warrants further exploration.

Certain genes are associated with pathogenesis of CKD. For example, the activation of the transcriptional regulator STAT3 has been reported in tubular cells following kidney
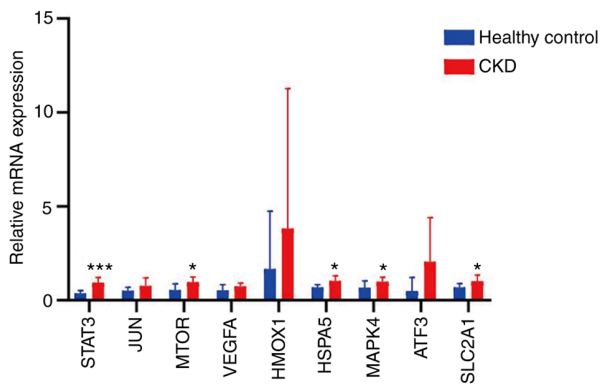
Figure 14. RNA levels of the top nine ferroptosis-associated genes measured in CKD and healthy kidney tissue. RNA levels of STAT3, JUN, MTOR, VEGF, HMOX1, HSPA5, MAPK14, ATF3 and SLC2A1 were compared via reverse transcription-quantitative PCR analysis of kidney tissue. *P<0.05 and ***P<0.001 vs. healthy control. Data are presented as the mean ± standard deviation and comparisons were performed using the two-sided unpaired Student's t test. CKD, chronic kidney disease; VEGF, vascular endothelial-derived growth factor; HMOX1, heme oxygenase 1; HSPA5, heat shock protein A5; ATF3, activation transcription factor 3; SLC2A1, solute carrier family 2 member 1.

damage, consistent with a potential role for STAT3 as a driver of CKD (41). Wang *et al* (42) suggested a role for mTOR as a mediator of CKD pathogenesis and that treatment with mTOR inhibitor rapamycin suppresses this signalling activity to protect against CKD. In a diabetic nephropathy model, HSPA5 has also been reported to be upregulated, with similar findings in UUO-induced renal fibrosis model (43,44). To the best of our knowledge, although no prior reports have specifically analysed SLC2A1 or MAPK14 in the context of CKD, knocking down MAPK14 promotes downregulation of cell division cycle 25B and suppresses clear cell renal cell carcinoma proliferative and migratory activity (45). In addition, GLUT1 deficiency syndrome is linked to the translational initiation of SLC2A1 via upstream regulatory mechanisms (46). The precise mechanistic pathways by which these verified genes affect development and progression of CKD, however, remain unclear. In the present analysis, RT-qPCR revealed that CKD was associated with upregulation of STAT3, MAPK14, HSPA5, MTOR and SLC2A1. Further investigation exploring genes downregulated in CKD is thus warranted.

Studies have highlighted the importance of ferroptotic cell death as a contributing factor to CKD incidence. For example, a recent study utilizing the UUO-induced renal fibrosis model system demonstrated that regulation of ferroptotic signalling can protect against renal damage (47). Wang *et al* (48) observed the induction of ferroptotic activity in a 5/6 nephrectomy-induced (one whole kidney is removed and the poles of the remaining kidney are ablated) CKD model and determined that dysregulated iron metabolism promotes this deleterious activity. Accordingly, the use of ferroptosis-inhibiting compounds, such as deferoxamine or ferrostatin-1, can protect against interstitial fibrosis, renal damage and accumulation of inflammatory cells in IRI or UUO-induced mice (7,49). In a UUO-induced renal fibrosis mouse model, tocilizumab mimotope treatment protects against renal injury and fibrotic activity by inhibiting ferroptosis (47). Together, these data highlight the key role of ferroptosis in pathogenic progression of CKD.

PBMC populations include multipotent progenitor cells that give rise to a diverse array of immune cell types, thereby coordinating both physiological and pathological immunological activity (50). Many immunosuppressive agents have been used for immune-mediated renal disease such as acute kidney injury, CKD and graft-versus-host disease (51). Immunosuppressor use in CKD is still under debate because only patients exhibiting large amounts of proteinuria will receive these treatments to balance the benefit and risks of immunosuppression (51). Preliminary data indicated that ferroptosis may induce immune cell-induced cell death (52,53). System xc⁻ (an exchange agency) levels are decreased in response to IFNγ (52), which is secreted by CD8⁺ T cells was recently reported to be involved in increasing tumour cell sensitivity towards ferroptosis. Another report revealed that IL-4 and IL-13 inhibit the expression of GPX4 in kidney cells and other cell types, corresponding to increased ALOX15 expression, thus allowing a robust generation of inflammatory arachidonic acid metabolites (53). The present study systematically analysed differential expression of immune cells and DFGs in CKD. DFGs in CKD were primarily associated with naive CD4⁺ T cells, Tregs, monocytes, neutrophils, resting and activated NK cells and activated dendritic cells.

However, the current study had limitations. Firstly, the amount of data analysed was small from the GSE15072 dataset and bioinformatics findings were obtained from blood samples and not kidney tissue of patients with CKD. Secondly, the clinical information downloaded from the GSE15072 dataset is incomplete, especially demographic data and clinical index, which may be helpful to understand the basic clinical features of patients with CKD and HD. Thirdly, experimental verification was performed on the kidney tissue of CKD rats; the present data need to be further verified in a higher number of CKD clinical samples. Moreover, the underlying mechanisms of ferroptosis and CKD, as well as the dysregulated genes in CKD and HD, need to be further demonstrated. However, potential therapeutic target genes and pathways were screened via bioinformatics, which may provide a theoretical foundation for further studies on therapeutic interventions, although clinical validation of these results is critical.

Altogether, the present findings suggested STAT3, MAPK14, HSPA5, MTOR and SLC2A1 as potential diagnostic and therapeutic biomarkers for CKD, providing evidence regarding the key role of ferroptosis in CKD.

Acknowledgements

Funding

Availability of data and materials

All data generated or analyzed during this study are included in this published article.

Authors' contributions

LS, CB and JW conceived the study. LS and QF confirm the authenticity of all the raw data. LS, YanZ and CS performed the experiments. QF and YaZ analyzed the data. LS wrote the manuscript. JW wrote and edited the manuscript. CB edited the manuscript. All authors have read and approved the final manuscript.

Ethics approval and consent to participate

The present study was approved by the Animal Ethical and Welfare Committee of Kunming Medical University (approval no. Kmmu20221379).

Patient consent for publication

Not applicable.

Competing interests

The authors declare that they have no competing interests.

References

1. Foreman K, Marquez N, Dolgert A, Fukutaki K, Fullman N, McGaughey M, Pletcher MA, Smith AE, Tang K, Yuan CW, *et al*: Forecasting life expectancy, years of life lost, and all-cause and cause-specific mortality for 250 causes of death: Reference and alternative scenarios for 2016-40 for 195 countries and territories. Lancet 392: 2052-2090, 2018.
2. Zhao H, Ma SX, Shang YQ, Zhang HQ and Su W: microRNAs in chronic kidney disease. Clin Chim Acta 491: 59-65, 2019.
3. Saritas T and Floege J: Cardiovascular disease in patients with chronic kidney disease. Herz 45: 122-128, 2020.
4. Sun Y, Chen P, Zhai B, Zhang M, Xiang Y, Fang J, Xu S, Gao Y, Chen X, Sui X and Li G: The emerging role of ferroptosis in inflammation. Biomed Pharmacother 127: 110108, 2020.
5. Battaglia A, Chirillo R, Aversa I, Sacco A, Costanzo F and Biamonte F: Ferroptosis and cancer: Mitochondria meet the 'Iron Maiden' cell death. Cells 9: 1505, 2020.
6. Zhang X and Li X: Abnormal iron and lipid metabolism mediated ferroptosis in kidney diseases and its therapeutic potential. Metabolites 12: 58, 2022.
7. Zhou L, Xue X, Hou Q and Dai C: Targeting ferroptosis attenuates interstitial inflammation and kidney fibrosis. Kidney Dis (Basel) 8: 57-71, 2022.
8. Moore JH: Bioinformatics. J Cell Physiol 213: 365-369, 2007.
9. Chen JY, Youn E and Mooney SD: Connecting protein interaction data, mutations, and disease using bioinformatics. Methods Mol Biol 541: 449-461, 2009.
10. Wang D, Xie N, Gao W, Kang R and Tang D: The ferroptosis inducer erastin promotes proliferation and differentiation in human peripheral blood mononuclear cells. Biochem Biophys Res Commun 503: 1689-1695, 2018.
11. Altintas M, DiBartolo S, Tadros L, Samelko B and Wasse H: Metabolic changes in peripheral blood mononuclear cells isolated from patients with end stage renal disease. Front Endocrinol (Lausanne) 12: 629239, 2021.
12. Hartman ML, Shirihai OS, Holbrook M, Xu G, Kocherla M, Shah A, Fetterman JL, Kluge MA, Frame AA, Hamburg M and Vita JA: Relation of mitochondrial oxygen consumption in peripheral blood mononuclear cells to vascular function in type 2 diabetes mellitus. Vasc Med 19: 67-74, 2014.
13. Calton EK, Keane KN, Raizel R, Rowlands J, Soares MJ and Newsholme P: Winter to summer change in vitamin D status reduces systemic inflammation and bioenergetic activity of human peripheral blood mononuclear cells. Redox Biol 12: 814-820, 2017.
14. Tomas C, Brown A, Strassheim V, Elson JL, Newton J and Manning P: Cellular bioenergetics is impaired in patients with chronic fatigue syndrome. PLoS one 12: e0186802, 2017.
15. Gangcuangco L, Mitchell BI, Siriwardhana C, Kohorn LB, Chew GM, Bowler S, Kallianpur KJ, Chow DC, Ndhlovu LC, Gerschenson M and Shikuma CM: Mitochondrial oxidative phosphorylation in peripheral blood mononuclear cells is decreased in chronic HIV and correlates with immune dysregulation. PLoS One 15: e0231761, 2020.
16. Gentleman RC, Carey VJ, Bates DM, Bolstad B, Dettling M, Dudoit S, Ellis B, Gautier L, Ge Y, Gentry J, *et al*: Bioconductor: Open software development for computational biology and bioinformatics. Genome Biol 5: R80, 2004.
17. Huber W, Carey VJ, Gentleman R, Anders S, Carlson M, Carvalho BS, Bravo HC, Davis S, Gatto L, Girke T, *et al*: Orchestrating high-throughput genomic analysis with Bioconductor. Nat Methods 12: 115-121, 2015.
18. Preisendorfer RW and Mobley CD: Principal component analysis in meteorology and oceanography. Journal 1988.
19. Ito K and Murphy D: Application of ggplot2 to pharmacometric graphics. CPT Pharmacometrics Syst Pharmacol 2: e79, 2013.
20. Zhou N and Bao J: FerrDb: A manually curated resource for regulators and markers of ferroptosis and ferroptosis-disease associations. Database (Oxford) 1: baaa021, 2020.
21. Jia A, Xu L and Wang Y: Venn diagrams in bioinformatics. Brief Bioinform 22: bbab108, 2021.
22. Wang JH, Zhao LF, Lin P, Su XR, Chen SJ, Huang LQ, Wang HF, Zhang H, Hu ZF, Yao KT and Huang ZX: GenCLiP 2.0: A web server for functional clustering of genes and construction of molecular networks based on free terms. Bioinformatics 30: 2534-2536, 2014.
23. Du J, Yuan Z, Ma Z, Song J, Xie X and Chen Y: KEGG-PATH: Kyoto encyclopedia of genes and genomes-based pathway analysis using a path analysis model. Mol Biosyst 10: 2441-2447, 2014.
24. Newman AM, Liu CL, Green MR, Gentles AJ, Feng W, Xu Y, Hoang CD, Diehn M and Alizadeh AA: Robust enumeration of cell subsets from tissue expression profiles. Nat Methods 12: 453-457, 2015.
25. Smoot ME, Ono K, Ruscheinski J, Wang PL and Ideker T: Cytoscape 2.8: New features for data integration and network visualization. Bioinformatics 27: 431-432, 2011.
26. Sandberg K and Umans JG: Recommendations concerning the new U.S. National institutes of health initiative to balance the sex of cells and animals in preclinical research. FASEB J 29: 1646-1652, 2015.
27. Livak KJ and Schmittgen TD: Analysis of relative gene expression data using real-time quantitative PCR and the 2(-Delta Delta C(T)) method. Methods 25: 402-408, 2001.
28. Viechtbauer W: Conducting meta-analyses in R with the metafor package. J Statistical Software 36: 1-48, 2010.
29. Masseroli M, Mons B, Bongcam-Rudloff E, Ceri S, Kel A, Rechenmann F, Lisacek F and Romano P: Integrated bio-search: Challenges and trends for the integration, search and comprehensive processing of biological information. BMC Bioinformatics 15 (Suppl 1): S2, 2014.
30. van Raaij S, van Swelm R, Bouman K, Cliteur M, van den Heuvel MC, Pertijs J, Patel D, Bass P, van Goor H, Unwin R, *et al*: Tubular iron deposition and iron handling proteins in human healthy kidney and chronic kidney disease. Sci Rep 8: 9353, 2018.
31. Liu Y: Epithelial to mesenchymal transition in renal fibrogenesis: Pathologic significance, molecular mechanism, and therapeutic intervention. J Am Soc Nephrol 15: 1-12, 2004.
32. Kalluri R and Neilson EG: Epithelial-mesenchymal transition and its implications for fibrosis. J Clin Invest 112: 1776-1784, 2003.
33. Chevalier RL: Pathogenesis of renal injury in obstructive uropathy. Curr Opin Pediatr 18: 153-160, 2006.
34. Zhao H, Han Y, Jiang N, Li C, Yang M, Xiao Y, Wei L, Xiong X, Yang J, Tang C, *et al*: Effects of HIF-1α on renal fibrosis in cisplatin-induced chronic kidney disease. Clin Sci (Lond) 135: 1273-1288, 2021.
35. Hillmer EJ, Zhang H, Li HS and Watowich SS: STAT3 signaling in immunity. Cytokine Growth Factor Rev 31: 1-15, 2016.
36. Zhou B, Liu J, Kang R, Klionsky DJ, Kroemer G and Tang D: Ferroptosis is a type of autophagy-dependent cell death. Semin Cancer Biol 66: 89-100, 2020.
37. Hirota Y, Yamashita S, Kurihara Y, Jin X, Aihara M, Saigusa T, Kang D and Kanki T: Mitophagy is primarily due to alternative autophagy and requires the MAPK1 and MAPK14 signaling pathways. Autophagy 11: 332-343, 2015.

38. Gomer C, Ferrario A, Rucker N, Wong S and Lee AS: Glucose regulated protein induction and cellular resistance to oxidative stress mediated by porphyrin photosensitization. Cancer Res 51: 6574-6579, 1991.
39. Saxton RA and Sabatini DM: MTOR signaling in growth, metabolism, and disease. Cell 168: 960-976, 2017.
40. Waln O and Jankovic J: Paroxysmal movement disorders. Neurol Clin 33: 137-152, 2015.
41. Bienaimé F, Muorah M, Yammine L, Burtin M, Nguyen C, Baron W, Garbay S, Viau A, Broueilh M, Blanc T, et al: Stat3 controls tubulointerstitial communication during CKD. J Am Soc Nephrol 27: 3690-3705, 2016.
42. Wang J, Chai L, Lu Y, Lu H, Liu Y and Zhang Y: Attenuation of mTOR signaling is the major response element in the rescue pathway of chronic kidney disease in rats. Neuroimmunomodulation 27: 9-18, 2020.
43. Lindenmeyer MT, Rastaldi MP, Ikehata M, Neusser MA, Kretzler M, Cohen CD and Schlöndorff D: Proteinuria and hyperglycemia induce endoplasmic reticulum stress. J Am Soc Nephrol 19: 2225-2236, 2008.
44. Bhreathnach U, Griffin B, Brennan E, Ewart L, Higgins D and Murphy M: Profibrotic IHG-1 complexes with renal disease associated HSPA5 and TRAP1 in mitochondria. Biochim Biophys Acta Mol Basis Dis 1863: 896-906, 2017.
45. Liu J, Yu X, Yu H, Liu B, Zhang Z, Kong C and Li Z: Knockdown of MAPK14 inhibits the proliferation and migration of clear cell renal cell carcinoma by downregulating the expression of CDC25B. Cancer Med 9: 1183-1195, 2020.
46. Willemsen MA, Vissers LE, Verbeek MM, van Bon BW, Geuer S, Gilissen C, Klepper J, Kwint MP, Leen WG, Pennings M, et al: Upstream SLC2A1 translation initiation causes GLUT1 deficiency syndrome. Eur J Hum Genet 25: 771-774, 2017.
47. Yang L, Guo J, Yu N, Liu Y, Song H, Niu J and Gu Y: Tocilizumab mimotope alleviates kidney injury and fibrosis by inhibiting IL-6 signaling and ferroptosis in UUO model. Life Sci 261: 118487, 2020.
48. Wang J, Wang Y, Liu Y, Cai X, Huang X, Fu W, Wang L, Qiu L, Li J and Sun L: Ferroptosis, a new target for treatment of renal injury and fibrosis in a 5/6 nephrectomy-induced CKD rat model. Cell Death Discov 8: 127, 2022.
49. Ikeda Y, Ozono I, Tajima S, Imao M, Horinouchi Y, Izawa-Ishizawa Y, Kihira Y, Miyamoto L, Ishizawa K, Tsuchiya K and Tamaki T: Iron chelation by deferoxamine prevents renal interstitial fibrosis in mice with unilateral ureteral obstruction. PLoS One 9: e89355, 2014.
50. Zhang M and Huang B: The multi-differentiation potential of peripheral blood mononuclear cells. Stem Cell Res Ther 3: 48, 2012.
51. Tang P, Zhang Y, Chan M, Lam WWY, Chung JYF, Kang W, To KF, Lan HY and Tang PMK: The emerging role of innate immunity in chronic kidney diseases. Int J Mol Sci 21: 4018, 2020.
52. Sato H, Fujiwara K, Sagara J and Bannai S: Induction of cystine transport activity in mouse peritoneal macrophages by bacterial lipopolysaccharide. Biochem J 310: 547-551, 1995.
53. Schnurr K, Borchert A and Kuhn H: Inverse regulation of lipid-peroxidizing and hydroperoxyl lipid-reducing enzymes by interleukins 4 and 13. FASEB J 13: 143-154, 1999.